



Cite this: *J. Mater. Chem. A*, 2022, 10, 20111

## Synthesis, crystal structure, and properties of stoichiometric hard tungsten tetraboride, $\text{WB}_4$ †

Elena Bykova,<sup>a,b</sup> Sergey V. Ovsyannikov,<sup>a</sup> Maxim Bykov,<sup>c</sup> Yuqing Yin,<sup>de</sup> Timofey Fedotenko,<sup>f</sup> Hendrik Holz,<sup>gh</sup> Stefan Gabel,<sup>h</sup> Benoit Merle,<sup>gh</sup> Stella Chariton,<sup>i</sup> Vitali B. Prakapenka,<sup>i</sup> Natalia Dubrovinskaia,<sup>dj</sup> Alexander F. Goncharov,<sup>b</sup> and Leonid Dubrovinsky<sup>a</sup>

Tungsten tetraboride has been known so far as a non-stoichiometric compound with a variable composition (e.g.  $\text{WB}_{4-x}$ ,  $\text{WB}_{4+x}$ ). Its mechanical properties could exceed those of hard tungsten carbide, which is widely used nowadays in science and technology. The existence of stoichiometric  $\text{WB}_4$  has not been proven yet, and its structure and crystal chemistry remain debatable to date. Here we report the synthesis of single crystals of the stoichiometric  $\text{WB}_4$  phase under high-pressure high-temperature conditions. The crystal structure of  $\text{WB}_4$  was determined using synchrotron single-crystal X-ray diffraction. *In situ* high-pressure compressibility measurements show that the bulk modulus of  $\text{WB}_4$  is 238.6(2) GPa for  $B' = 5.6(0)$ . Measurements of mechanical properties of bulk polycrystalline sub-millimeter size samples under ambient conditions reveal a hardness of  $\sim 36$  GPa, confirming that the material falls in the category of superhard materials.

Received 21st March 2022

Accepted 9th August 2022

DOI: 10.1039/d2ta02268k

rsc.li/materials-a

<sup>a</sup>Bayerisches Geoinstitut, University of Bayreuth, Universitätsstrasse 30, D-95447, Bayreuth, Germany. E-mail: knilav@gmail.com

<sup>b</sup>Earth and Planets Laboratory, Carnegie Institution for Science, 5241 Broad Branch Road, NW, Washington DC, 20015, USA

<sup>c</sup>Institute of Inorganic Chemistry, University of Cologne, Greinstrasse 6, 50939 Cologne, Germany

<sup>d</sup>Material Physics and Technology at Extreme Conditions, Laboratory of Crystallography, University of Bayreuth, 95440 Bayreuth, Germany

<sup>e</sup>State Key Laboratory of Crystal Materials, Shandong University, Jinan 250100, China

<sup>f</sup>Photon Science, Deutsches Elektronen-Synchrotron, Notkestrasse 85, 22607 Hamburg, Germany

<sup>g</sup>Institute of Materials Engineering, University of Kassel, Mönchebergstr. 3, 34125 Kassel, Germany

<sup>h</sup>Materials Science & Engineering, Institute I, Friedrich-Alexander-Universität Erlangen-Nürnberg, Martensstr. 5, 91058 Erlangen, Germany

<sup>i</sup>Center for Advanced Radiation Sources, The University of Chicago, 5640 S. Ellis, Chicago, IL, 60637, USA

<sup>j</sup>Department of Physics, Chemistry and Biology (IFM), Linköping University, SE-58183 Linköping, Sweden

† Electronic supplementary information (ESI) available. CCDC 2158520–2158531 and 2158536. For ESI and crystallographic data in CIF or other electronic format see <https://doi.org/10.1039/d2ta02268k>



Elena Bykova received her PhD from Bayerisches Geoinstitut, University of Bayreuth, Germany. She worked as a postdoctoral researcher at the Extreme Conditions Beamline at the PETRA III synchrotron (Germany) and at Earth & Planets Laboratory, Carnegie Institution for Science (USA). Her research interests are mainly focused on developing methodologies of single-crystal X-ray diffraction experiments at high pressures and temperatures, in order to study materials related to mineral physics and materials sciences. In 2018, in recognition of her outstanding achievements in the field of ultra-high-pressure crystallography, she received the Max von Laue Prize from the German Crystallographic Society.

## Introduction

Inexpensive hard and superhard (with a Vickers hardness of around 40 GPa and above) materials are in much demand for various industrial applications. Novel carbides,<sup>1</sup> nitrides,<sup>2–8</sup> borides,<sup>9–23</sup> and other compounds of transition metals,<sup>24,25</sup> which can potentially combine high hardness and promising optical, electronic, and other properties, are the focus of extensive investigations.<sup>26–28</sup> Nowadays, one of the most widely used hard materials for commercial applications is tungsten carbide, WC. This fact motivates investigations of other potentially hard tungsten compounds, primarily, borides.<sup>29–37</sup> Among them, a phase referred to as “WB<sub>4</sub>”,<sup>38–49</sup> and its several derivatives (e.g., W<sub>1–x</sub>B<sub>3</sub>, WB<sub>4–x</sub>, WB<sub>4+x</sub>, WB<sub>4.2</sub>, and WB<sub>5–x</sub>)<sup>50–56</sup> were identified as highly promising candidates, whose mechanical characteristics (e.g. theoretical and experimental values of  $H_V$  vary from 30 to 45 GPa (ref. 26,44,45,47,49 and 54)) could exceed those of WC (Vickers hardness  $H_V \sim 18$ –20 GPa (ref. 57)). However, the crystal chemistry of the “WB<sub>4</sub>” phase has remained debatable for decades, and thus, often, it is not clear what material is being considered in a particular publication.

Based on high-quality powder diffraction data, several probable structural models for the “WB<sub>4</sub>” phase were suggested (hexagonal unit cell,  $a \sim 5.20$  Å,  $c \sim 6.34$  Å, Fig. 1a–d).<sup>38,39,42–45,47,58</sup> In contrast, theoretical calculations suggested an alternative crystal structure for “WB<sub>4</sub>” (sp.gr.  $P6_3/mmc$ ,  $a \sim 2.93$ – $2.96$  Å,  $c \sim 10.9$ – $11.0$  Å, Fig. 1f),<sup>31,36,37,48</sup> but it has not been experimentally observed to date.

Recently, one more boron-rich phase, WB<sub>5</sub> was first predicted (sp. gr.  $Pmmn$ ,  $a = 6.369$ ,  $b = 5.199$ ,  $c = 8.993$  Å, Fig. 1e)<sup>34</sup> and then synthesized in the form of two boron-deficient phases, WB<sub>4.18</sub> and WB<sub>4.86</sub>.<sup>54</sup> Crystal structures of these WB<sub>5</sub>, WB<sub>4.18</sub> and WB<sub>4.86</sub> phases were found to be very similar to those reported earlier for the seemingly “WB<sub>4</sub>” phase and its derivatives.<sup>38,39,42</sup> This finding may suggest that: (i) the stoichiometric WB<sub>5</sub> phase is actually the “parent” for the family of boron-deficient phases

WB<sub>5–x</sub> ( $0 \leq x < 1.6$ ) reported to date; (ii) a genuine stoichiometric WB<sub>4</sub> phase for which a different crystal structure was predicted<sup>31,36,37,48</sup> probably has not been synthesized yet, and previous claims of its synthesis were likely due to confusion with one of the WB<sub>5–x</sub> phases.<sup>54</sup>

In this work, we report the first synthesis of single crystals of the so far “elusive” stoichiometric WB<sub>4</sub> phase and an accurate determination of its crystal structure by single-crystal X-ray diffraction. In order to synthesize the phase, we first performed a fast screening of chemical reactivity of the W–B system up to 30 GPa and then scaled-up the amount of the WB<sub>4</sub> phase using a multi-anvil apparatus. We find that a crystal structure of the genuine WB<sub>4</sub> phase indeed differs from previous experimentally-determined models for the seemingly “WB<sub>4</sub>” phase,<sup>26,38,39,42,44,45,47,49,59</sup> while, it is well consistent with the one predicted for WB<sub>4</sub>.<sup>31,36,37,48</sup> Examinations of mechanical properties of the single- and polycrystalline samples of WB<sub>4</sub> confirm the hard nature of this phase.

## Experimental procedures

### Synthesis of WB<sub>4</sub> single crystals in diamond anvil cells

For high-pressure high-temperature experiments, we have used a BX90 type DAC<sup>60</sup> equipped with Boehler-Almax diamonds with a 200 µm culet size (60° opening angle). In between diamonds, we placed a rhenium gasket pre-indented to 25 µm thickness with a hole of about 100 µm in diameter that served as a pressure chamber. Inside the pressure chamber, we placed a thin tungsten plate sandwiched between pre-compressed amorphous boron powder together with a small ruby sphere (for pressure estimation). Neon was used both as a pressure transmitting medium and as a pressure standard.<sup>61</sup>

The laser-heating coupled with XRD measurements were conducted at the 13-IDB beamline at the Advanced Photon Source, Argonne National Laboratory (Pilatus CdTe 1M detector, X-ray wavelength  $\lambda = 0.2952$  Å, focal spot  $\sim 3$  µm).<sup>62</sup>

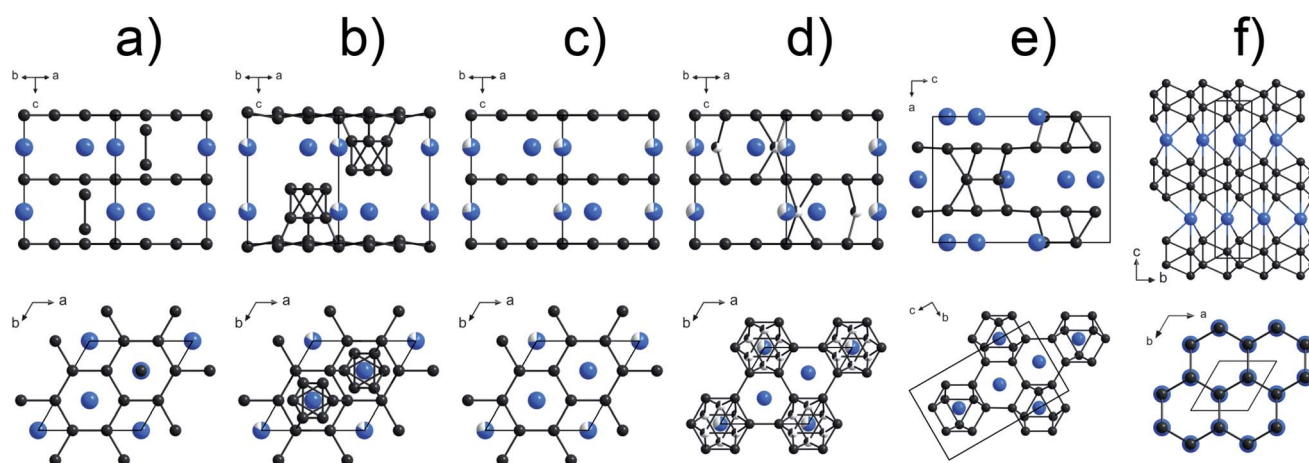


Fig. 1 Various models of the crystal structure proposed for WB<sub>4</sub>: (a) the crystal structure of WB<sub>4</sub> by Romans and Krug;<sup>39</sup> (b) W<sub>1.83</sub>B<sub>9</sub> by Nowotny et al.;<sup>58</sup> (c) W<sub>1–x</sub>B<sub>3</sub> following Lundström and Rosenberg<sup>59</sup> and Zeiringer et al.;<sup>42</sup> (d) WB<sub>4.2</sub> by Lech et al.;<sup>47</sup> (e) WB<sub>5</sub> by Kvashnin et al.;<sup>34,54</sup> (f) theoretically predicted stoichiometric WB<sub>4</sub>.<sup>31,36,37,48</sup> The blue spheres represent tungsten atoms, the black spheres are boron atoms, and the partially filled spheres indicate defect B or W sites.

The sample-to-detector distance, coordinates of the beam center, tilt angle and tilt plane rotation angle of the detector images were calibrated using NIST LaB<sub>6</sub>. Lasers were focused down to a flat top of about 10 μm in diameter. The sample temperature was measured by the standard spectroradiometry method<sup>63</sup> using an Acton SP-2360 imaging spectrograph coupled with a PI-MAX3 1024i ICCD camera from Princeton Instruments. Pressure values and maximum heating temperatures are given in Table S1.†

After each laser heating cycle, a detailed X-ray diffraction map was collected around the heated spot in order to determine the phase composition of the reaction product. At each pressure point, single-crystal XRD images were collected in different spots with the decent quality of the diffraction data (up to six data collection procedures) in order to determine phase composition of the reaction product. The single-crystal XRD images were recorded while rotating the sample about a single  $\omega$ -axis from  $-30$  to  $+30^\circ$  in small steps of  $0.5^\circ$ .

The DIOPTAS software<sup>64</sup> was used for preliminary phase analysis and calculation of pressures from the positions of the XRD lines of Ne. Powder XRD patterns were analyzed using a JANA2020, where the unit cell parameters of the phases in the multi-phase mixtures were refined from the full-profile Le Bail fit.<sup>65</sup>

### Synthesis of WB<sub>4</sub> single crystals in multi-anvil assemblies

The WB<sub>4</sub> samples were synthesized under high-pressure high-temperature (HP-HT) conditions using multi-anvil presses at the Bayerisches Geoinstitut (BGI).<sup>66</sup> Typically, the samples were synthesized at 20 GPa under heating at 1800–2000 °C for several hours (Table S1†). We used standard multi-anvil assemblies with LaCrO<sub>3</sub>-heaters and W3Re/W25Re thermocouples for temperature determination. Sample capsules were prepared from 50 μm thick tungsten foil (99.95% purity, HMW Hauner GmbH & Co. KG company). We followed several synthetic routes, including mixing of fine powders of tungsten and boron and mixing of tungsten foil with boron powder. The latter allowed fabrication of microscopic single crystals at the border of the tungsten foil; whereas, the former could fabricate relatively large polycrystals. Besides the above tungsten foil, we used tungsten powder (99.9% purity, Chempur company) for mixing with boron powder. In preliminary testing syntheses, we used a powder of amorphous boron (95–97% purity, Chempur company), while for synthesis of chemically pure samples, we ground into powder the  $\beta$ -boron crystals (99.5% purity, Chempur company). Structural and chemical analyses of the samples were performed by X-ray diffraction using a three-circle Bruker diffractometer (SMART APEX CCD detector, Incoatec I $\mu$ S 3.0 microfocus X-ray source, Ag-K $\alpha$  radiation), and by scanning electron microscopy (SEM) using a LEO-1530 instrument, respectively. Other details and procedures were similar to those described before.<sup>67,68</sup>

### Measurements of single-crystal compressibility

A single crystal of WB<sub>4</sub> (black, plate-shape,  $10 \times 10 \times 5 \mu\text{m}^3$ ) pre-selected on an in-house single-crystal diffractometer was loaded in a membrane-driven BX90 type DAC equipped with

Boehler-Almax diamonds with a 250 μm culet size ( $60^\circ$  opening angle, Re gasket). A small ruby sphere and a Ne pressure-transmitting medium were used for pressure determination. The WB<sub>4</sub> crystal in the diamond anvil cell was compressed to about 54 GPa with a pressure step of 1–4 GPa. The single-crystal XRD pattern of the sample was measured at each pressure point (narrow  $\omega$ -scanning from  $-30$  to  $+30^\circ$ ,  $0.5^\circ$  steps).

The XRD experiments were conducted at the Extreme Conditions Beamline P02.2 at PETRA III, Hamburg, Germany (PerkinElmer XRD1621 flat panel detector,  $\lambda = 0.2900 \text{ \AA}$ , KB-mirror focusing, focal spot  $\sim 3 \mu\text{m}$ ). The sample-to-detector distance, coordinates of the beam center, tilt angle and tilt plane rotation angle of the detector images were calibrated using CeO<sub>2</sub>.

### Single-crystal X-ray diffraction

The single-crystal XRD data (the unit cell determination, integration of the reflection intensities, and empirical absorption correction) were processed using the CrysAlisPro software.<sup>69</sup> In the cases of multi-phase and multi-grain samples (which, for instance, are being formed after laser heating), we manually searched for peaks belonging to the most intense grains using the reciprocal space Ewald explorer implemented in CrysAlisPro. After the unit cell indexing, the unit cell and orientation matrix obtained were used for further data integration.

A single crystal of orthoenstatite ((Mg<sub>1.93</sub>,Fe<sub>0.06</sub>)(Si<sub>1.93</sub>,Al<sub>0.06</sub>)O<sub>6</sub>, *Pbca*,  $a = 18.2391(3)$ ,  $b = 8.8117(2)$ , and  $c = 5.18320(10) \text{ \AA}$ ) was used to calibrate the instrument model of CrysAlisPro (the sample-to-detector distance, the detector's origin, offsets of the goniometer angles, rotation of the X-ray beam and the detector around the instrument axis).

The crystal structures were determined by using SHELXT,<sup>70</sup> a structure solution program that uses the method of intrinsic phasing. The crystal structure was refined against  $F^2$  on all data using full-matrix least-squares with the SHELXL<sup>71</sup> software. SHELXT and SHELXL programs were implemented in the Olex2 software package.<sup>72</sup> Since the body of the diamond anvil cell shadows more than 50% of the diffraction reflections, the reflection datasets were incomplete. In order to improve the data/parameter ratio, only atomic thermal parameters of tungsten were refined in anisotropic approximation. Another refinement strategy where boron atoms have been also refined anisotropically with a RIGU rigid-bond restraint gave no significant improvements in  $R_1/wR_2$  values but rather brought a problem with elongated/negative ADPs for most B atoms; therefore, it was not applied.

A detailed summary of the crystal structure refinements together with the unit cell parameters, atomic coordinates and isotropic displacement parameters is given in Table S2.† The X-ray crystallographic coordinates have been deposited at the Inorganic Crystal Structure Database (ICSD), and the deposition numbers are given in Table S2.†.

### Measurements of the hardness and Young's modulus

Nanoindentation was performed using a Nanoindenter G200 platform (KLA, Milpitas, CA, USA), equipped with a Berkovich diamond tip (Synton MDP, Nidau, Switzerland) and by the

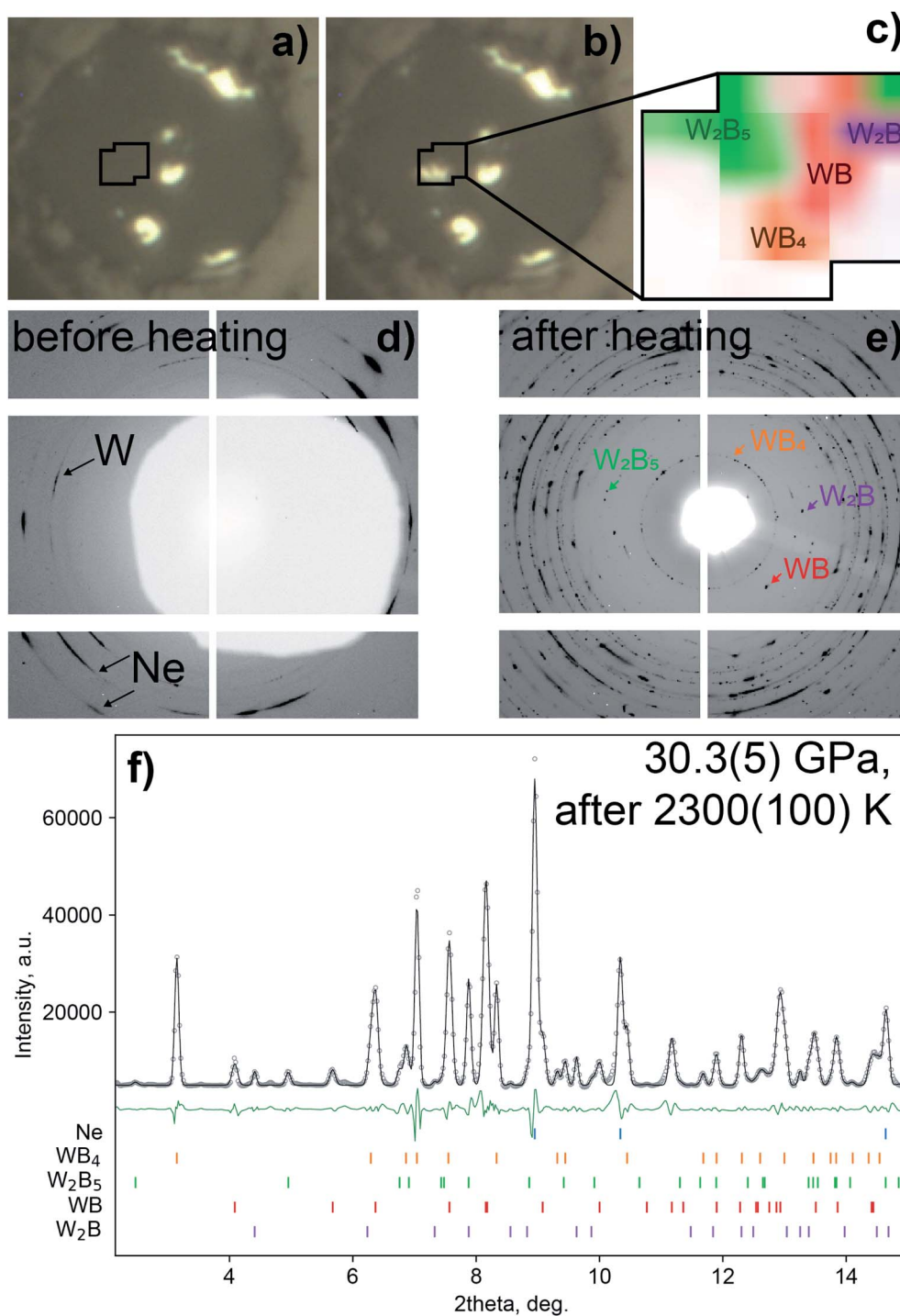


**Fig. 2** Synthesis of tungsten borides at high pressure. Microscopic images of the pressure chamber before (a) and after (b) the laser heating at 30.3(5) GPa, and the inset (c) shows phase distribution around the heated area obtained by X-ray diffraction mapping of the heated area. By using a combination of powder and single-crystal XRD methods, four borides of tungsten were identified in the pressure chamber, namely,  $WB_4$ ,  $W_2B_5$ ,  $WB$  and  $W_2B$ . Corresponding fragments of 2D diffraction images in the low- $2\theta$  region show diffraction peaks before (d) and after a laser heating (e). A white area at (d) is a shadow from a beam stop to block scattering from X-ray transparent glassy carbon mirrors used for on-axis laser heating. The lower image (f) shows the powder X-ray diffraction data collected at 30.3(5) GPa after a laser heating of up to 2300(100) K ( $\lambda = 0.2952 \text{ \AA}$ ): the experimental data are shown by grey circles (the background was subtracted), a Le Bail fit – by the black solid line, and a difference curve – by the green solid line; the ticks show predicted positions of the diffraction peaks. The Le Bail fit showing profiles of the individual phases is given in supplementary Fig. S2.†



continuous stiffness method (CSM).<sup>73</sup> The indents were separated by a distance of at least 10  $\mu\text{m}$ , so that their plastic zones did not overlap.<sup>74</sup> The indentations were performed on different areas of the sample, which respectively appeared homogeneous and heterogeneous in the optical micrographs as can be seen in Fig. S1,<sup>†</sup> and are assumed to be single crystalline and polycrystalline, and the size of the single crystalline areas could reach 30 microns. All in all, 20 measurements were performed. For each test, loading was performed at a constant strain-rate of  $0.1\text{ s}^{-1}$  up to a maximal indentation depth of at least 900 nm. A 2 nm large CSM oscillation superimposed at 41 Hz on the loading signal was used to continuously measure the hardness and Young's modulus with increasing indentation depth. The acquired data were evaluated using the Oliver–Pharr method.<sup>75,76</sup> For this purpose, the diamond punch geometry was calibrated in fused

silica, and the machine frame stiffness correction was refined so as to obtain a constant stiffness-squared-over-load ratio during indentation on the samples. The mechanical properties were averaged over the indentation depth range 700–900 nm in order to minimize tip blunting effects at shallow depth. The conversion of the reduced moduli to Young's moduli was performed assuming a Poisson's ratio of 0.2 for  $\text{WB}_4$ .<sup>31</sup> The conversion from the nanoindentation hardness  $H_{\text{IT}}$  to the Vickers hardness  $H_{\text{V}}$  was carried out with a factor of 0.9269.<sup>77</sup>

## Results and discussion

### Synthesis of single crystals and polycrystals

Single crystals and polycrystals of  $\text{WB}_4$  were synthesized under high-pressure high-temperature (HP-HT) conditions using both

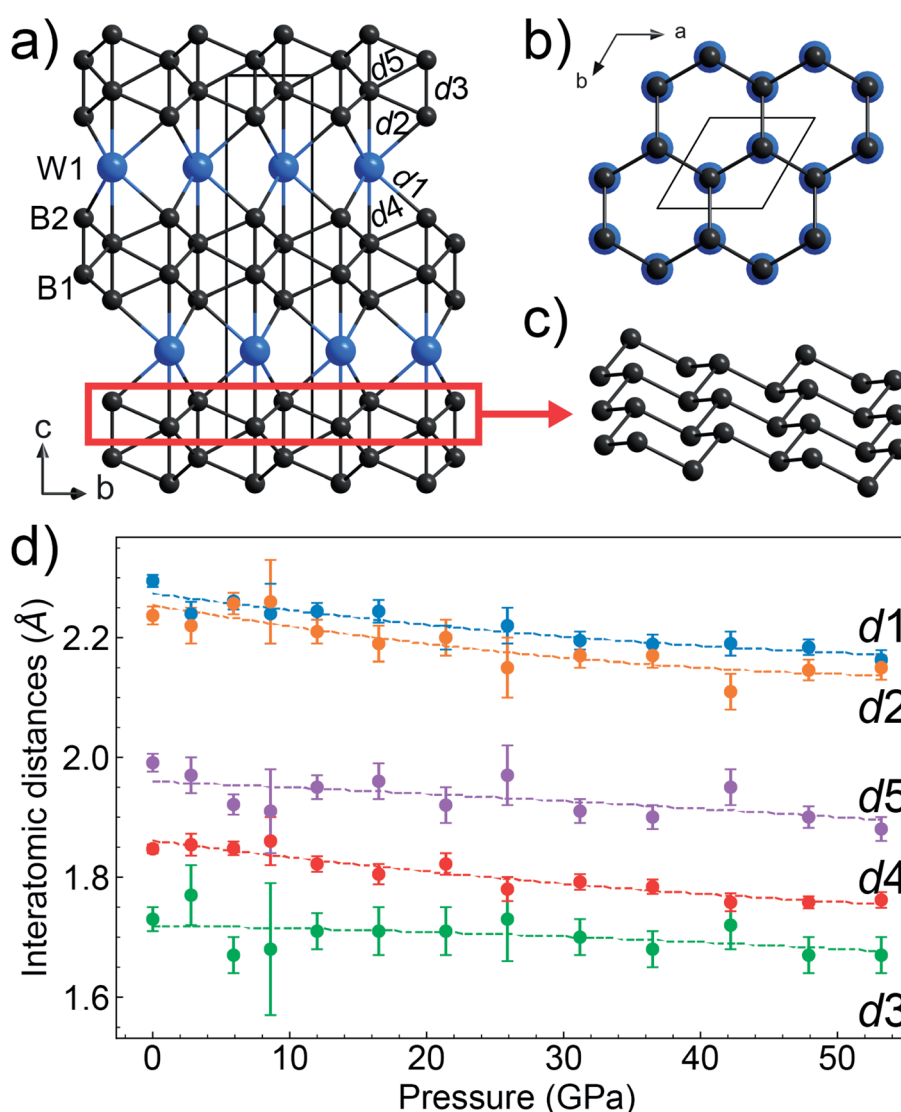


**Fig. 3** Crystal structure of  $\text{WB}_4$  projected down the  $a$ -axis (a) and  $c$ -axis (b). All structures consist of hexagonal layers of W atoms (blue spheres) interchanging with the network formed by covalently bonded boron atoms (black spheres). The red rectangle highlights a single puckered layer formed by condensed six-membered rings of boron in a chair-like conformation, and the layer in a different projection is shown in (c). Compressibility of interatomic distances and bonds in  $\text{WB}_4$  (d): d1, d2 –  $\text{W}\cdots\text{B}$  distances and d3–d5 –  $\text{B}\cdots\text{B}$  bonds. The solid symbols – data retrieved from the single-crystal diffraction measurements, and the dashed lines are the 2<sup>nd</sup>-order polynomial fits of compression data serving as a guide to the eye.

large-volume multi-anvil presses at BGI and laser-heated diamond anvil cells (DACs). In the experiments using the DAC, a  $\text{WB}_4$  phase (sp.gr.  $P6_3/mmc$ ,  $a = 2.8481(3) \text{ \AA}$ ,  $c = 10.752(2) \text{ \AA}$ ) was first detected at 30.3(5) GPa after a laser heating of up to 2300(100) K. As can be seen in Fig. 2, single crystals of  $\text{WB}_4$  are formed together with a  $\text{W}_2\text{B}$  phase (sp.gr.  $I4/mcm$ ,  $a = 5.4257(10) \text{ \AA}$ ,  $c = 4.6189(12) \text{ \AA}$ ),  $\text{WB}$  (sp.gr.  $I4_1/amd$ ,  $a = 3.0325(4) \text{ \AA}$ ,  $c = 16.558(3) \text{ \AA}$ ) and a phase with a R-centered hexagonal unit cell ( $a = 2.9143(5) \text{ \AA}$ ;  $c = 20.463(5) \text{ \AA}$ ). The latter lattice parameters belong to a tungsten boride for which two chemical compositions have been proposed, namely,  $\text{W}_2\text{B}_5$  (ref. 78) and  $\text{W}_2\text{B}_4$  (ref. 79 and 80) (below we use  $\text{W}_2\text{B}_5$  notation). Such a wide variety of the W : B ratios can be explained by a design of our DAC experiments. In the reaction chamber, tungsten foil was embedded between two pieces of pre-compressed boron powder, which results in inhomogeneous distribution of the reactants across the reaction chamber and their insufficient mixing. More boron-rich borides likely formed in the spots with local excess of boron, while borides with a larger W : B ratio formed in the boron-poor regions. We cannot exclude that thermal gradients typical of the laser heating (at least  $\pm 100 \text{ K}$ ) could lead to chemical variety of the resulting products.

In the multi-anvil experiments, tungsten tetraboride (as well as a byproduct,  $\text{WB}_2$ ) can be successfully synthesized at 20 GPa and 2073 K. It should be noted that no  $\text{WB}_5$  or any of its derivatives have been found among the reaction products neither in the multi-anvil nor in DAC experiments.

### Crystal structure and comparison with previous results

From the synthesis products, we selected high-quality single crystals of  $\text{WB}_4$  and determined their crystal structure by single-crystal X-ray diffraction (Fig. S3†). In the crystal structure of tungsten tetraboride (Fig. 3a and b), the metal atoms form the flat hexagonal close packed layers perpendicular to the  $c$ -axis that follow the ABABA... sequence. Covalently-bonded boron networks are located between layers of tungsten atoms. The networks consist of two puckered layers connected through short B–B bonds (notated as d3 in Fig. 3a). Such layers are formed by condensed six-membered rings of boron in a chair-like conformation, which one can find, for example, in grey arsenic (A7-type) and in a high-pressure modification of black phosphorus (Fig. 3c).<sup>81</sup> The crystal structure of  $\text{WB}_4$  demonstrates a close similarity to one of hard  $\text{ReB}_2$ , which has the same arrangement of metal atoms, while its boron network is formed only by a one puckered layer.<sup>82</sup> The single-crystal XRD data show that tungsten and boron atoms fully occupy their positions, leaving no vacancies. The crystal structure we experimentally determined fully agrees with theoretical predictions.<sup>31,36,37,48</sup>

Both early<sup>38,39</sup> and recent<sup>26,42,44,45,47,49</sup> experimental structural studies of the “ $\text{WB}_4$ ” phase proposed a different crystal structure, which is built from interchanging defect close-packed metal layers and planar boron honeycomb layers and interstitial boron atoms (Fig. 1a–e). A structural similarity to  $\text{WB}_5$  suggests that all the “ $\text{WB}_4$ ” phases reported in previous publications were, likely, boron-deficient  $\text{WB}_{5-x}$ , but not genuine stoichiometric  $\text{WB}_4$ .<sup>54</sup> Furthermore, it was predicted that the

genuine stoichiometric  $\text{WB}_4$  phase is thermodynamically stable only above 1 GPa,<sup>54</sup> and hence, ambient-pressure syntheses were unlikely to be capable to fabricate it.

### Mechanical properties

We examined the mechanical properties of our  $\text{WB}_4$  crystals by measurements of single-crystal compressibility using pressure-dependent single crystal X-ray diffraction up to 54 GPa (Fig. 4) and by measurements of both hardness and Young's modulus.

The high pressure *in situ* single crystal X-ray diffraction studies up to 54 GPa were carried out using a neon quasi-hydrostatic pressure-transmitting medium. The  $\text{WB}_4$  sample showed no phase transitions under compression up to 54 GPa, and we could follow pressure evolutions of its unit cell parameters. Fitting the third-order Birch–Murnaghan equation of state to the volumetric data, we estimated the bulk modulus to be  $B_0 = 238.6(2) \text{ GPa}$  for  $B' = 5.6(0)$  and  $B_0 = 262.5(2) \text{ GPa}$  for fixed  $B' = 4$  (Fig. 4). As seen from this plot, the  $\text{WB}_4$  crystal has a sizable difference in axial compressibility, and along the  $c$ -axis, it is the most incompressible. The shortest B–B bonds (denoted as d3 Fig. 3a) in the crystal structure are oriented along the  $c$ -axis and have the lowest compressibility compared to the other B–B bonds and  $\text{W}\cdots\text{B}$  contacts (Fig. 3d); therefore, we can expect that these bonds largely contribute to the axial incompressibility. The bulk modulus of  $\text{WB}_4$  appeared to be smaller than that for  $\text{WB}_{5-x}$  phases:  $B_0 \sim 304\text{--}342 \text{ GPa}$  with fixed  $B' = 4$  (see ref. 83 and refs therein). On the other hand, stoichiometric  $\text{WB}_4$  shows no lattice parameter softening around 42 GPa, as has been observed previously for a non-stoichiometric phase.<sup>83</sup>

### The hardness and Young's modulus

The nanoindentation hardness and Young's modulus measurements are shown in Fig. 5. In the likely single crystal-line areas, they returned average values of  $H_{\text{IT}} = 40.2(5) \text{ GPa}$



Fig. 4 Pressure dependencies of relative variations in the unit-cell volume and lattice parameters of a  $\text{WB}_4$  single crystal at 295 K. Error bars are smaller than symbols' size.

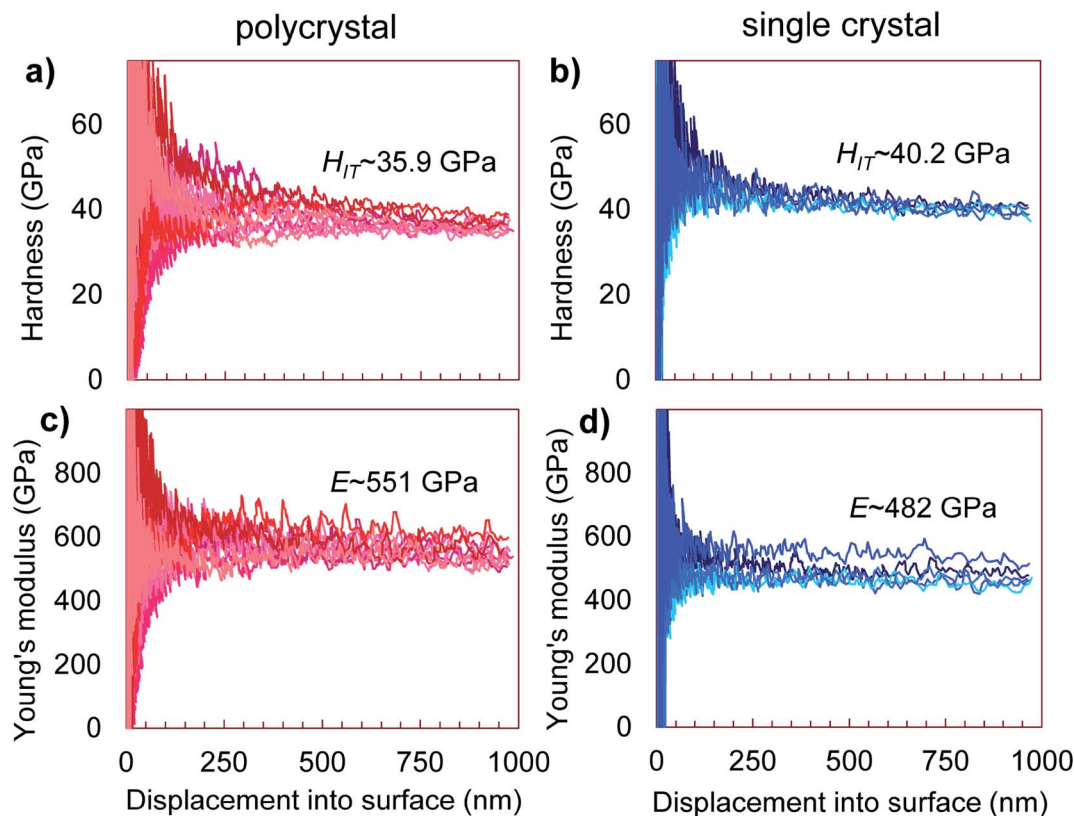


Fig. 5 The nanoindentation hardness,  $H_{IT}$  (a and b), and Young's modulus,  $E$  (c and d) of polycrystals (a and c) and single crystals (b and d) of  $WB_4$  at 295 K. Each plot combines several tests and shows average values.

(corresponding to  $H_V = 37.3(5)$  GPa) and  $E = 482(30)$  GPa. Likewise, for the likely polycrystalline area, the hardness was found to be  $H_{IT} = 35.9(1.6)$  GPa (corresponding to  $H_V =$

33.3(1.5) GPa) and the Young's modulus  $E = 551(24)$  GPa (Fig. 5). These magnitudes confirm that  $WB_4$  is a hard material and generally agrees with previous experimental estimations of

**Table 1** Mechanical properties of stoichiometric  $WB_4$  (isotropic bulk modulus  $B$ , shear modulus  $G$ , Young's modulus  $E$  and estimated values of Vickers' hardness  $H_V$ ; all units are in GPa) compared with reported literature values for various models of  $WB_4$ ,  $WB_5$  and their derivatives<sup>a</sup>

Phase	Space group		$B$	$G$	$B/G$	$E$	$H_V$	Reference
$hP10-WB_4$	$P6_3/mmc$	Exp.	262.5(2)	227(2)	1.16(1)	482(30)	37.3(5)	This work – single crystal
		Exp.	262.5(2)	214(5)	1.23(3)	551(24)	33.3(1.5)	This work – polycrystal
		Calc.	294	215	1.367	519	28–35 <sup>a</sup>	17
		Calc.	292	213	1.371	514	21.3 <sup>b</sup>	88
		Calc.	299	217	1.378	525	29.0 <sup>a</sup>	31
		Calc.	302	259	1.166	604	40.0 <sup>a</sup>	36
		Calc.	297	217	1.372	523	28.8 <sup>c</sup>	37
$hP15-WB_4$	$R-3m$	Calc.	299	137	2.182	356	11.3 <sup>a</sup>	31
		Calc.	308	253	1.217	596	37–42 <sup>a</sup>	17
$hP20-WB_4$	$P6_3/mmc$	Exp.	304(10)				46.2(1.2) <sup>f</sup>	26
		Exp.	339(3)			553(14)	43.3(2.9) <sup>f</sup>	44
		Calc.	392	104			41.1 <sup>d</sup>	43
		Calc.	328	129	2.543	325		29
		Calc.	300	102	2.941	274	5.2 <sup>a</sup>	89
$WB_{4.2}$ $WB_5$	$P6_3/mmc$ $P6mm$	Calc.	298	85	3.506	233	3.2 <sup>a</sup>	31
		Calc.	280	245	1.143	569	39.7 <sup>c</sup>	54
		Calc.	287	267	1.075	611	44.9 <sup>a</sup>	36
		Calc.	295	270	1.093	621	44.7 <sup>c</sup>	54
$WB_{5-x}-WB_2$ (50/50%)		Exp.					29.3(2.3) <sup>f</sup>	90
$WB_{5-x}-WB_2$ (67/33%)		Exp.					38.7(1.1) <sup>f</sup>	90

<sup>a</sup> Calculated using the empirical models of: a – Chen,<sup>85</sup> b – Šimůnek,<sup>91</sup> c – Tian,<sup>92</sup> d – Gao,<sup>93</sup> and e – Mazhnik–Oganov;<sup>94</sup> f – experimental hardness measured at an applied load of 0.49 N.

hardness for seemingly “WB<sub>4</sub>” (WB<sub>5-x</sub>) phases to be about  $H_V \sim 30\text{--}45$  GPa (ref. 26,44,45,47,49 and 54) (see Table 1 for comparison of mechanical properties). The elastic and plastic properties of hard solids are known to correlate with each other.<sup>84</sup> Given the above experimentally-determined values of the bulk modulus ( $B_0 = 262.5(2)$  for  $B = 4$ ) (Fig. 4) and hardness ( $H_V = 37.3(5)$  and  $33.3(1.5)$  GPa) (Fig. 5a and b) for single- and polycrystalline samples of WB<sub>4</sub>, one can calculate their shear moduli ( $G$ ) by using an empirical formula proposed by X. Q. Chen *et al.* and verified by numerous examples as follows:<sup>85,86</sup>

$$H_V^{\text{(Chen)}} = 2(k^2 G)^{0.585} - 3,$$

where  $k = G/B_0$ . The returned values of the shear moduli of  $G = 227(2)$  and  $214(5)$  GPa for single- and polycrystalline samples, respectively, are in a good agreement with the literature data (Table 1). The Pugh modulus ratios ( $B_0/G$ ) are 1.16(1) and 1.23(3), respectively. These values are much less than 1.75, – the threshold magnitude, which differentiates between brittle ( $B_0/G < 1.75$ ) and ductile ( $B_0/G > 1.75$ ) materials.<sup>87</sup> Hence, WB<sub>4</sub> is a brittle material and cannot be deformed in a ductile manner.

## Conclusions

We have successfully synthesized single crystals of the predicted but so far “elusive” stoichiometric WB<sub>4</sub> phase, determined its crystal structure by single-crystal X-ray diffraction and investigated its mechanical properties. A hexagonal crystal structure of stoichiometric tungsten tetraboride is formed by hexagonal close-packed single tungsten atom layers, which interchange with covalently-bonded boron two-layer networks with short B–B bonds along the *c*-axis. The latter bonds contribute to the anisotropic character of axial compressibility. Our single-crystal diffraction data suggest that tungsten atoms fully occupy their crystallographic positions, while no additional interstitial boron atoms with partial occupancy could be identified. *In situ* high-pressure study shows that the bulk modulus of WB<sub>4</sub> is 238.6(2) GPa. Measurements of mechanical properties of bulk polycrystalline samples under ambient conditions reveal a hardness of  $\sim 36$  GPa. Our work solved the long-standing challenge of the “WB<sub>4</sub>” phase and confirmed its high technological potential as a hard material. Further enhancement of its mechanical properties could be achieved by alloying with other elements, as it was demonstrated on a non-stoichiometric polymorph of WB<sub>4.2</sub>.<sup>44,47</sup> This phase allows hosting a wide variety of transition metals in its structure forming ternary alloys. As a result, its own Vickers microindentation hardness can increase from  $\sim 43$  GPa to 51–56 GPa by addition of 6–8% of Ti, Zr or Hf<sup>95</sup> and to 53–54 GPa by addition of 2–10 at% of Ta, Mn or Cr<sup>96</sup> (the values were measured under an applied load of 0.49 N). Incorporation of group III transition metals (Y and Sc) and selected lanthanoids (Gd, Tb, Dy, Ho, and Er) also improves hardness values and oxidation resistance.<sup>97</sup>

## Author contributions

Elena Bykova: investigation, conceptualization, formal analysis, funding acquisition, and writing – original draft; Sergey V.

Ovsyannikov: investigation, formal analysis, and writing – original draft; Maxim Bykov: investigation and writing – review & editing; Yuqing Yin: investigation; Timofey Fedotenko: investigation and data curation; Hendrik Holz: investigation and formal analysis; Stefan Gabel: investigation and formal analysis; Benoit Merle: investigation, formal analysis, and writing – original draft; Stella Chariton: investigation and data curation; Vitali B. Prakapenka: investigation, data curation, methodology, and writing – review & editing; Natalia Dubrovinskaya: resources and writing – review & editing; Alexander F. Goncharov: resources and writing – review & editing; Leonid Dubrovinsky: funding acquisition, resources, and writing – review & editing.

## Conflicts of interest

There are no conflicts to declare.

## Acknowledgements

E. B, M. B. and A. F. G. acknowledge support of the Carnegie Institution of Washington. E. B. acknowledges financial support from the program ‘Promotion of Equal Opportunities for Women in Research and Teaching’ funded by the Free State of Bavaria. M. B. acknowledges the support of Deutsche Forschungsgemeinschaft (DFG project BY112/2-1). Portions of this work were performed at GeoSoilEnviroCARS (The University of Chicago, Sector 13), Advanced Photon Source (APS), Argonne National Laboratory. GeoSoilEnviroCARS is supported by the National Science Foundation – Earth Sciences (EAR – 1634415). This research used resources of the Advanced Photon Source, a U.S. Department of Energy (DOE) Office of Science User Facility operated for the DOE Office of Science by Argonne National Laboratory under Contract No. DE-AC02-06CH11357. This research used resources from the Center for Nano-analysis and Electron Microscopy (CENEM) at Friedrich-Alexander University Erlangen-Nürnberg.

## References

- 1 Y. Liang, X.-F. Wei, C. Gu, J.-X. Liu, F. Li, M. Yan, X. Zheng, Z. Han, Y. Zhao, S. Wang, J. Yang, W. Zhang, L. Kou and G.-J. Zhang, *ACS Appl. Mater. Interfaces*, 2021, **13**, 14365–14376.
- 2 A. Zerr, R. Riedel, T. Sekine, J. E. Lowther, W. Y. Ching and I. Tanaka, *Adv. Mater.*, 2006, **18**, 2933–2948.
- 3 A. Zerr, G. Miehe, G. Serghiou, M. Schwarz, E. Kroke, R. Riedel, H. Fueß, P. Kroll and R. Boehler, *Nature*, 1999, **400**, 340–342.
- 4 K. Watanabe, T. Taniguchi and H. Kanda, *Nat. Mater.*, 2004, **3**, 404–409.
- 5 S. Vogel, A. T. Buda and W. Schnick, *Angew. Chemie Int. Ed.*, 2018, **57**, 13202–13205.
- 6 P. Wang, S. Wang, Y. Zou, J. Zhu, D. He, L. Wang and Y. Zhao, *Crystals*, 2021, **11**, 614.
- 7 M. Bykov, S. Chariton, H. Fei, T. Fedotenko, G. Aprilis, A. V. Ponomareva, F. Tasnádi, I. A. Abrikosov, B. Merle,



- P. Feldner, S. Vogel, W. Schnick, V. B. Prakapenka, E. Greenberg, M. Hanfland, A. Pakhomova, H.-P. Liermann, T. Katsura, N. Dubrovinskaia and L. Dubrovinsky, *Nat. Commun.*, 2019, **10**, 2994.
- 8 M. Bykov, E. Bykova, A. V. Ponomareva, I. A. Abrikosov, S. Chariton, V. B. Prakapenka, M. F. Mahmood, L. Dubrovinsky and A. F. Goncharov, *Angew. Chemie Int. Ed.*, 2021, **60**, 9003–9008.
- 9 B. Albert, *Angew. Chemie Int. Ed.*, 1998, **37**, 1117–1118.
- 10 H. Gou, L. Hou, J. Zhang, H. Li, G. Sun and F. Gao, *Appl. Phys. Lett.*, 2006, **88**, 221904.
- 11 B. Petermüller, C. Neun, K. Wurst, L. Bayarjargal, D. Zimmer, W. Morgenroth, M. Avalos-Borja, I. G. Becerril-Juarez, M. J. Mühlbauer, B. Winkler and H. Huppertz, *Inorg. Chem.*, 2018, **57**, 10341–10351.
- 12 B. Petermüller, C. Neun, M. Stekiel, D. Zimmer, M. Tribus, K. Wurst, B. Winkler and H. Huppertz, *Chem.-Eur. J.*, 2018, **24**, 14679–14685.
- 13 C. Neun, B. Petermüller, E. Haussühl, L. Bayarjargal, K. Wurst, T. Götsch, S. Penner, W. Morgenroth, I. G. Becerril-Juarez, M. Avalos-Borja, H. Huppertz and B. Winkler, *Solid State Sci.*, 2020, **105**, 106211.
- 14 H. Tang, X. Gao, J. Zhang, B. Gao, W. Zhou, B. Yan, X. Li, Q. Zhang, S. Peng, D. Huang, L. Zhang, X. Yuan, B. Wan, C. Peng, L. Wu, D. Zhang, H. Liu, L. Gu, F. Gao, T. Irifune, R. Ahuja, H.-K. K. Mao and H. Gou, *Chem. Mater.*, 2020, **32**, 459–467.
- 15 B. Zhao, X. Wang, L. Yu, Y. Liu, X. Chen, B. Yang, G. Yang, S. Zhang, L. Gu and X. Liu, *Adv. Funct. Mater.*, 2022, **32**, 2110872.
- 16 H.-Y. Chung, M. B. Weinberger, J.-M. Yang, S. H. Tolbert and R. B. Kaner, *Appl. Phys. Lett.*, 2008, **92**, 261904.
- 17 H. Gou, Z. Li, H. Niu, F. Gao, J. Zhang, R. C. Ewing and J. Lian, *Appl. Phys. Lett.*, 2012, **100**, 111907.
- 18 H. Gou, N. Dubrovinskaia, E. Bykova, A. A. Tsirlin, D. Kasinathan, W. Schnelle, A. Richter, M. Merlini, M. Hanfland, A. M. Abakumov, D. Batuk, G. Van Tendeloo, Y. Nakajima, A. N. Kolmogorov and L. Dubrovinsky, *Phys. Rev. Lett.*, 2013, **111**, 157002.
- 19 A. Knappschneider, C. Litterscheid, D. Dzivenko, J. A. Kurzman, R. Seshadri, N. Wagner, J. Beck, R. Riedel and B. Albert, *Inorg. Chem.*, 2013, **52**, 540–542.
- 20 A. Knappschneider, C. Litterscheid, N. C. George, J. Brgoch, N. Wagner, J. Beck, J. A. Kurzman, R. Seshadri and B. Albert, *Angew. Chem. Int. Ed.*, 2014, **53**, 1684–1688.
- 21 H. Gou, A. A. Tsirlin, E. Bykova, A. M. Abakumov, G. Van Tendeloo, A. Richter, S. V. Ovsyannikov, A. V. Kurnosov, D. M. Trots, Z. Konôpková, H.-P. Liermann, L. Dubrovinsky and N. Dubrovinskaia, *Phys. Rev. B: Condens. Matter Mater. Phys.*, 2014, **89**, 064108.
- 22 E. Bykova, A. A. Tsirlin, H. Gou, L. Dubrovinsky and N. Dubrovinskaia, *J. Alloys Compd.*, 2014, **608**, 69–72.
- 23 G. Akopov, M. T. Yeung and R. B. Kaner, *Adv. Mater.*, 2017, **29**, 1604506.
- 24 S. B. Schneider, D. Baumann, A. Salamat, Z. Konôpková, H.-P. Liermann, M. R. Schwarz, W. Morgenroth, L. Bayarjargal, A. Friedrich, B. Winkler and W. Schnick, *Chem. Mater.*, 2012, **24**, 3240–3246.
- 25 B. Fuchs, D. Johrendt, L. Bayarjargal and H. Huppertz, *Angew. Chemie Int. Ed.*, 2021, **60**, 21801–21806.
- 26 Q. Gu, G. G. Krauss and W. Steurer, *Adv. Mater.*, 2008, **20**, 3620–3626.
- 27 G. Akopov, L. E. Pangilinan, R. Mohammadi and R. B. Kaner, *APL Mater.*, 2018, **6**, 070901.
- 28 Z. Zhang, A. Mansouri Tehrani, A. O. Oliynyk, B. Day and J. Brgoch, *Adv. Mater.*, 2021, **33**, 2005112.
- 29 E. Zhao, J. Meng, Y. Ma and Z. Wu, *Phys. Chem. Chem. Phys.*, 2010, **12**, 13158.
- 30 Q. Tao, D. Zheng, X. Zhao, Y. Chen, Q. Li, Q. Li, C. Wang, T. Cui, Y. Ma, X. Wang and P. Zhu, *Chem. Mater.*, 2014, **26**, 5297–5302.
- 31 X.-Y. Cheng, X.-Q. Chen, D.-Z. Li and Y.-Y. Li, *Acta Crystallogr. Sect. C Struct. Chem.*, 2014, **70**, 85–103.
- 32 T. Moscicki, J. Radziejewska, J. Hoffman, J. Chrzanowska, N. Levintant-Zayonts, D. Garbiec and Z. Szymanski, *Ceram. Int.*, 2015, **41**, 8273–8281.
- 33 N. G. Szwacki, *Sci. Rep.*, 2017, **7**, 1–6.
- 34 A. G. Kvashnin, H. A. Zakaryan, C. Zhao, Y. Duan, Y. A. Kvashnina, C. Xie, H. Dong and A. R. Oganov, *J. Phys. Chem. Lett.*, 2018, **9**, 3470–3477.
- 35 Z. Qin, W. Gong, X. Song, M. Wang, H. Wang and Q. Li, *RSC Adv.*, 2018, **8**, 35664–35671.
- 36 C. Zhao, Y. Duan, J. Gao, W. Liu, H. H. Dong, H. H. Dong, D. Zhang and A. R. Oganov, *Phys. Chem. Chem. Phys.*, 2018, **20**, 24665–24670.
- 37 A. Yang, Y. Duan, M. Peng, L. Shen and H. Qi, *Appl. Phys. A*, 2022, **128**, 152.
- 38 A. Chretien and J. Helgorsky, *CR*, 1961, **252**, 742–744.
- 39 P. A. Romans and M. P. Krug, *Acta Crystallogr.*, 1966, **20**, 313–315.
- 40 J. Dong, H. Li, J. Wang, Z. Guo, J. Liao, X. Hao, X. Zhang and D. Chen, *J. Phys. Chem. C*, 2019, **123**, 29314–29323.
- 41 Y. Wang, Y. Wu, Y. Lu, X. Wang, Y. Duan and M. Peng, *Vacuum*, 2022, **196**, 110731.
- 42 I. Zeiringer, P. Rogl, A. Grytsiv, J. Polt, E. Bauer and G. Giester, *J. Phase Equilibria Diffus.*, 2014, **35**, 384–395.
- 43 M. Wang, Y. Li, T. Cui, Y. Ma and G. Zou, *Appl. Phys. Lett.*, 2008, **93**, 101905.
- 44 R. Mohammadi, A. T. Lech, M. Xie, B. E. Weaver, M. T. Yeung, S. H. Tolbert and R. B. Kaner, *Proc. Natl. Acad. Sci.*, 2011, **108**, 10958–10962.
- 45 J. V. Rau, A. Latini, R. Teghil, A. De Bonis, M. Fosca, R. Caminiti and V. Rossi Albertini, *ACS Appl. Mater. Interfaces*, 2011, **3**, 3738–3743.
- 46 X.-L. Wu, X.-L. Zhou and J. Chang, *Int. J. Mod. Phys. B*, 2015, **29**, 1550103.
- 47 A. T. Lech, C. L. Turner, R. Mohammadi, S. H. Tolbert and R. B. Kaner, *Proc. Natl. Acad. Sci.*, 2015, **112**, 3223–3228.
- 48 X. Li, Y. Tao and F. Peng, *J. Alloys Compd.*, 2016, **687**, 579–585.
- 49 G. Akopov, M. T. Yeung, I. Roh, Z. C. Sobell, H. Yin, W. H. Mak, S. I. Khan and R. B. Kaner, *Chem. Mater.*, 2018, **30**, 3559–3570.

- 50 H. Gou, Z. Li, L.-M. Wang, J. Lian and Y. Wang, *AIP Adv.*, 2012, **2**, 012171.
- 51 X. Cheng, W. Zhang, X.-Q. Chen, H. Niu, P. Liu, K. Du, G. Liu, D. Li, H.-M. Cheng, H. Ye and Y. Li, *Appl. Phys. Lett.*, 2013, **103**, 171903.
- 52 E. M. Carnicom, J. Strychalska-Nowak, P. Wiśniewski, D. Kaczorowski, W. Xie, T. Klimczuk and R. J. Cava, *Supercond. Sci. Technol.*, 2018, **31**, 115005.
- 53 W. Gong, C. Liu, X. Song, Q. Li, Y. Ma and C. Chen, *Phys. Rev. B*, 2019, **100**, 220102.
- 54 A. G. Kvashnin, D. V. Rybkovskiy, V. P. Filonenko, V. I. Bugakov, I. P. Zibrov, V. V. Brazhkin, A. R. Oganov, A. A. Osipov and A. Y. Zakirov, *Adv. Sci.*, 2020, **7**, 2000775.
- 55 C. Gu, Y. Liang, X. Zhou, J. Chen, D. Ma, J. Qin, W. Zhang, Q. Zhang, L. L. Daemen, Y. Zhao and S. Wang, *Phys. Rev. B*, 2021, **104**, 014110.
- 56 K. D. Shumilov, Z. Mehmedović, H. Yin, P. Poths, S. Nuryyeva, I. Liepuoniute, C. Jang, I. Winardi and A. N. Alexandrova, *J. Phys. Chem. C*, 2021, **125**, 9486–9496.
- 57 F. Cardarelli, *Materials Handbook. A Concise Desktop Reference*, Springer London, London, 2nd edn, 2008.
- 58 H. Nowotny, H. Haschke and F. Benesovsky, *Monatshefte für Chemie – Chem. Mon.*, 1967, **98**, 547–554.
- 59 T. Lundström and I. Rosenberg, *J. Solid State Chem.*, 1973, **6**, 299–305.
- 60 R. Letoullec, J. P. Pinceaux and P. Loubeyre, *High Press. Res.*, 1988, **1**, 77–90.
- 61 Y. Fei, A. Ricolleau, M. Frank, K. Mibe, G. Shen and V. Prakapenka, *Proc. Natl. Acad. Sci. U. S. A.*, 2007, **104**, 9182–9186.
- 62 V. B. Prakapenka, A. Kubo, A. Kuznetsov, A. Laskin, O. Shkurikhin, P. Dera, M. L. Rivers and S. R. Sutton, *High Press. Res.*, 2008, **28**, 225–235.
- 63 D. L. Heinz and R. Jeanloz, in *High-Pressure Research in Mineral Physics: A Volume in Honor of Syun-iti Akimoto*, ed. M. H. Manghnani and Y. Syono, Terra Scientific Publishing, 1987, vol. 39, pp. 113–127.
- 64 C. Prescher and V. B. Prakapenka, *High Press. Res.*, 2015, **35**, 223–230.
- 65 V. Petříček, M. Dušek and L. Palatinus, *Zeitschrift für Krist. – Cryst. Mater.*, 2014, **229**, 345–352.
- 66 D. Frost, B. Poe, R. Trønnes, C. Liebske, A. Duba and D. Rubie, *Phys. Earth Planet. Inter.*, 2004, **143–144**, 507–514.
- 67 S. V. Ovsyannikov, M. Bykov, S. A. Medvedev, P. G. Naumov, A. Jesche, A. A. Tsirlin, E. Bykova, I. Chuvashova, A. E. Karkin, V. Dyadkin, D. Chernyshov and L. S. Dubrovinsky, *Angew. Chem., Int. Ed.*, 2020, **59**, 5632–5636.
- 68 S. V. Ovsyannikov, H. Gou, A. E. Karkin, V. V. Shchennikov, R. Wirth, V. Dmitriev, Y. Nakajima, N. Dubrovinskaia and L. S. Dubrovinsky, *Chem. Mater.*, 2014, **26**, 5274–5281.
- 69 CrysAlisPro Softw, *Syst. version 1.171.40.84a*, Rigaku Oxford Diffraction, Oxford, UK.
- 70 G. M. Sheldrick, *Acta Crystallogr. Sect. A Found. Adv.*, 2015, **71**, 3–8.
- 71 G. M. Sheldrick, *Acta Crystallogr. Sect. C Struct. Chem.*, 2015, **71**, 3–8.
- 72 O. V. Dolomanov, L. J. Bourhis, R. J. Gildea, J. A. K. Howard and H. Puschmann, *J. Appl. Crystallogr.*, 2009, **42**, 339–341.
- 73 B. Merle, V. Maier-Kiener and G. M. Pharr, *Acta Mater.*, 2017, **134**, 167–176.
- 74 P. Sudharshan Phani and W. C. Oliver, *Mater. Des.*, 2019, **164**, 107563.
- 75 W. C. Oliver and G. M. Pharr, *J. Mater. Res.*, 1992, **7**, 1564–1583.
- 76 W. C. Oliver and G. M. Pharr, *J. Mater. Res.*, 2004, **19**, 3–20.
- 77 Metallic materials—Instrumented indentation test for hardness and materials parameters—Part 1: Test method. Int. Stand. ISO 14577–1, 2002.
- 78 R. Kiessling, A. Wetterholm, L. G. Sillén, A. Linnasalmi and P. Laukkanen, *Acta Chem. Scand.*, 1947, **1**, 893–916.
- 79 M. Kayhan, E. Hildebrandt, M. Frotscher, A. Senyshyn, K. Hofmann, L. Alff and B. Albert, *Solid State Sci.*, 2012, **14**, 1656–1659.
- 80 M. Frotscher, W. Klein, J. Bauer, C.-M. Fang, J.-F. Halet, A. Senyshyn, C. Baetz and B. Albert, *Zeitschrift für Anorg. und Allg. Chemie*, 2007, **633**, 2626–2630.
- 81 J. C. Jamieson, *Science*, 1963, **139**, 1291–1292.
- 82 H.-Y. Y. Chung, M. B. Weinberger, J. B. Levine, A. Kavner, J.-M. M. Yang, S. H. Tolbert and R. B. Kaner, *Science*, 2007, **316**, 436–439.
- 83 M. Xie, R. Mohammadi, Z. Mao, M. M. Armentrout, A. Kavner, R. B. Kaner and S. H. Tolbert, *Phys. Rev. B: Condens. Matter Mater. Phys.*, 2012, **85**, 1–8.
- 84 D. M. Teter, *MRS Bull.*, 1998, **23**, 22–27.
- 85 X. Q. Chen, H. Niu, D. Li and Y. Li, *Intermetallics*, 2011, **19**, 1275–1281.
- 86 X.-Q. Chen, H. Niu, C. Franchini, D. Li and Y. Li, *Phys. Rev. B: Condens. Matter Mater. Phys.*, 2011, **84**, 121405.
- 87 S. F. Pugh, *Dublin Philos. Mag. J. Sci.*, 1954, **45**, 823–843.
- 88 M. Zhang, H. Yan, Q. Wei and H. Wang, *Comput. Mater. Sci.*, 2013, **68**, 371–378.
- 89 Y. Liang, Z. Fu, X. Yuan, S. Wang, Z. Zhong and W. Zhang, *Europhys. Lett.*, 2012, **98**, 66004.
- 90 A. Y. Pak, D. V. Rybkovskiy, Y. Z. Vassilyeva, E. N. Kolobova, A. V. Filimonenko and A. G. Kvashnin, *Inorg. Chem.*, 2022, **61**, 6773–6784.
- 91 A. Šimůnek and J. Vackář, *Phys. Rev. Lett.*, 2006, **96**, 085501.
- 92 Y. Tian, B. Xu and Z. Zhao, *Int. J. Refract. Met. Hard Mater.*, 2012, **33**, 93–106.
- 93 F. Gao, J. He, E. Wu, S. Liu, D. Yu, D. Li, S. Zhang and Y. Tian, *Phys. Rev. Lett.*, 2003, **91**, 015502.
- 94 E. Mazhnik and A. R. Oganov, *J. Appl. Phys.*, 2019, **126**, 125109.
- 95 G. Akopov, M. T. Yeung, C. L. Turner, R. Mohammadi and R. B. Kaner, *J. Am. Chem. Soc.*, 2016, **138**, 5714–5721.
- 96 M. Xie, R. Mohammadi, C. L. Turner, R. B. Kaner, A. Kavner and S. H. Tolbert, *Appl. Phys. Lett.*, 2015, **107**, 041903.
- 97 G. Akopov, M. T. Yeung, I. Roh, Z. C. Sobell, H. Yin, W. H. Mak, S. I. Khan and R. B. Kaner, *Chem. Mater.*, 2018, **30**, 3559–3570.